

Triassic Nb-enriched basalts, magnesian andesites, and adakites of the Qiangtang terrane (Central Tibet): evidence for metasomatism by slab-derived melts in the mantle wedge

Qiang Wang · Derek A. Wyman · Jifeng Xu · Yusheng Wan ·
Chaofeng Li · Feng Zi · Ziqi Jiang · Huaning Qiu · Zhuyin Chu ·
Zhenhua Zhao · Yanhui Dong

Received: 20 May 2007 / Accepted: 7 September 2007 / Published online: 17 October 2007
© Springer-Verlag 2007

Abstract New chronological, geochemical, and isotopic data are reported for Triassic (219–236 Ma) adakite-magnesian andesite-Nb-enriched basaltic rock associations from the Tuotuohe area, central Qiangtang terrane. The adakites and magnesian andesites are characterized by high Sr/Y (25–45), La/Yb (14–42) and Na₂O/K₂O (12–49) ratios, high Al₂O₃ (15.34–18.28 wt%) and moderate to high Sr concentrations (220–498 ppm) and $\varepsilon_{\text{ND}}(t)$ (+0.86 to +1.21) values. Low enrichments of Th, Rb relative to Nb, and subequal normalized Nb and La contents, and enrichments of light rare earth elements combine to distinguish a group of Nb-enriched basaltic rocks (NEBs). They have positive $\varepsilon_{\text{ND}}(t)$ (+2.57 to +5.16) values. Positive correlations between Th, La and Nb and an absence of negative Nb anomalies on mantle normalized plots indicate the NEBs are products of a mantle source metasomatized by a slab

melt rather than by hydrous fluids. A continuous compositional variation between adakites and magnesian andesites confirms slab melt interaction with mantle peridotite. The spatial association of the NEBs with adakites and magnesian andesites define an “adakitic metasomatic volcanic series” recognized in many demonstrably subduction-related environments (e.g., Mindanao arc, Philippines; Kamchatka arc, Russia; and southern Baja California arc, Mexico). The age of the Tuotuohe suite, and its correlation with Triassic NEB to the north indicates that volcanism derived from subduction-modified mantle was abundant prior to 220 Ma in the central Qiangtang terrane.

Keywords Adakite · Nb-enriched basalt · Magnesian andesite · Triassic · Subduction zone · Tibet

Communicated by H. Keppler.

Q. Wang · J. Xu · F. Zi · Z. Jiang · H. Qiu · Z. Zhao · Y. Dong
Key Laboratory of Isotope Geochronology and Geochemistry,
Guangzhou Institute of Geochemistry,
Chinese Academy of Sciences, Guangzhou 510640,
People's Republic of China

D. A. Wyman (✉)
School of Geosciences, Division of Geology and Geophysics,
The University of Sydney, Sydney, NSW 2006, Australia
e-mail: dwyman@geosci.usyd.edu.au

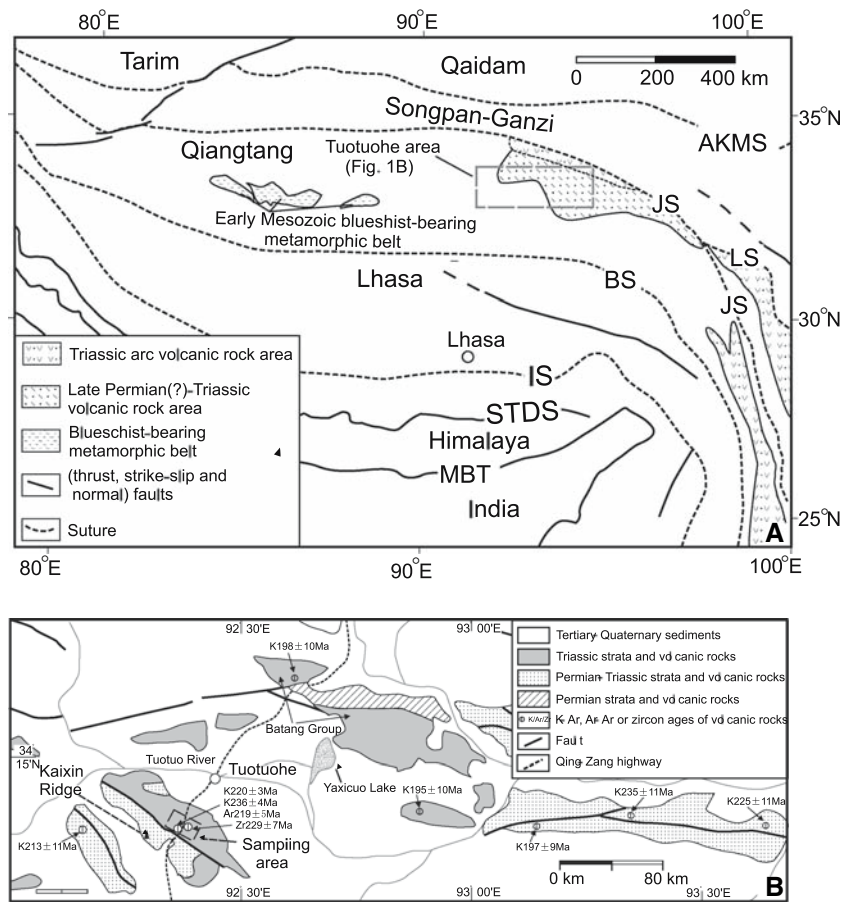
Y. Wan
Geological Institute, Chinese Academy of Geological Sciences,
Beijing 100037, People's Republic of China

C. Li · Z. Chu
Institute of Geology and Geophysics,
Chinese Academy of Sciences, Beijing 100029,
People's Republic of China

Introduction

The Triassic tectonic evolution of Central Tibet has attracted widespread interest because of the presence of a >500-km-long and up to 100-km-wide Paleozoic–Triassic blueschist (or eclogite)-bearing metamorphic belt (or Triassic melange) in the central Qiangtang terrane (e.g., Li et al. 1995; Kapp et al. 2000, 2003; Yin and Harrison 2000; Zhang 2001; Zhang et al. 2006a, b). Kapp et al. (2000, 2003) argued that its protolith from the Songpan-Ganzi block or oceanic basin was underthrust ~200 km southward beneath the Qiangtang terrane during Triassic flat subduction of the Paleo-Tethyan oceanic lithosphere along the Jinshajiang suture. The blueschist (or eclogite)-bearing metamorphic rocks were contemporarily generated and then exhumed in an intracontinental setting from depths of 35–50 km to upper crustal levels in <12 Ma by Late

Fig. 1 **a** Map of the Tibetan plateau showing major Terranes and temporal-spatial distribution of Late Permian (?)–Triassic volcanic rocks [modified from diagrams of Yin and Harrison (2000), Pan and Ding (2004) and Chung et al. (2005)]. Main suture zones between major Terranes: *AKMS* Anyimaqen-Kunlun-Muztagh, *JS* Jinshajiang and *LS* Litang, *BS* Bangong, *IS* Indus. Major faults: *STDS* southern Tibet detachment system; *MBT* Main Boundary thrust. **b** Simplified geologic map showing outcrops of Triassic volcanic rocks in the Tuotuohe area, Qiangtang terrane, central Tibet [after Pan and Ding (2004)]. The geochronological data for volcanic rocks are from Zhang and Zheng (1994)



Triassic–Early Jurassic crust-scale normal detachment faulting during continued early Mesozoic subduction. The Kapp et al. (2000, 2003) model predicts that: (1) significant portions of the central Tibetan continental mantle lithosphere were removed during Triassic flat subduction; (2) there was no Triassic magmatic arc in the Qiangtang terrane and no mantle wedge beneath the terrain; and (3) the deeper crust of central Tibet mainly consists of Triassic accretionary melange, and related Cenozoic in situ melts. The latter prediction contrasts with other proposals that partial melting of autochthonous and Proterozoic (>0.9 Ga) continental lithosphere may have generated the shoshonitic or high-K magmas, which are characteristic of Cenozoic volcanic rocks in central Tibet (e.g., Turner et al. 1996).

Other researchers contend that the Qiangtang melange developed in situ, based on arguments that the suture separates distinct fossil fauna types, alternative stratigraphic interpretations, and geochemical data (Li et al. 1995; Zhang 2001; Zhang et al. 2006a). For example, Zhang et al. (2006a) concluded that the compositions of metasiliciclastic rocks and metabasalts of the Qiangtang metamorphic belt did not correlate with those of the Jinshajiang suture. Rather than representing underthrust equivalents of the Jinshajiang suture, Zhang et al. (2006a)

argue that the Qiangtang metamorphic belt must have developed in place. Accordingly, the issue of Triassic low-angle Paleo-Tethyan subduction represents a key point of contention for Mesozoic–Cenozoic tectonic models of central Tibet. This paper reports on a study of igneous rocks in the Qiangtang terrane that provide an important new perspective on the nature of the Triassic subduction and the extent of subduction-related magmatism in the region.

Early reconnaissance studies concluded that the volcanic rocks to the south of the town of Tuotuohe (Fig. 1), located to the northeast of the blueschist (or eclogite)-bearing metamorphic belt, were produced in a Late Permian intracontinental rift (Dewey et al. 1988; Pearce and Mei 1988; Kapp et al. 2003) and those to the north of Tuotuohe were related to a Triassic oceanic arc or an arc developed on thinned continental lithosphere (Pearce and Mei 1988). Based on fossil evidence documented in later field surveys and a regional tectonic synthesis, Hsü et al. (1995) concluded that Permian and Triassic volcanic rocks occurred both to the south and north of Tuotuohe and that they all originated from southward subduction of Paleotethys oceanic lithosphere. More recent geochronological data (see below) confirm that Triassic volcanic rocks occur south of Tuotuohe and they are considered by Pan and Ding (2004)

and Zhang and Zheng (1994) to have been generated in an arc setting.

This paper presents new geochronological and geochemical data for volcanic rocks to the south of Tuotuohe. These data demonstrate that the rocks have Triassic ages and consist of NEBs-magnesian andesites-adakites, which are similar to the adakite metasomatic arc volcanic series identified in the Phillipines, Mexico, Kamchatka and elsewhere (e.g., Defant and Kepezhinskas 2001). The occurrence of this association in the central Qiantang places important constraints on subduction processes along the Jinshajiang suture zone.

Geological setting

The Qiantang terrane is one of three main east-west trending continental terranes of the Tibetan plateau (Fig. 1a; Yin and Harrison 2000; Pan and Ding 2004; Chung et al. 2005). It is bounded to the north by the Jinshajiang suture and a subordinate offset in the eastern Qiantang terrane: the Litang suture. It is generally accepted that accretion of the Songpan-Ganzi and Qiantang terranes along this suture occurred in the Triassic and that subduction was to the south (Dewey et al. 1988; Yin and Harrison 2000). To the south, the Qiantang terrane is bounded by the Banggong suture where suturing with the Lhasa terrane is generally considered to have occurred during the late Jurassic (Dewey et al. 1988; Yin and Harrison 2000).

Volcanic rocks of the central Qiantang terrane (Fig. 1a) include those of the Batang Group, which are located 25–40 km north and northeast of Tuotuohe and are underlain by Triassic conglomerates, sandstones, and minor carbonate units (Fig. 1b). The volcanic rocks are directly overlain by Triassic (Norian age: 206–216 Ma) marine carbonates (Pearce and Mei 1988; Leeder et al. 1988), which is consistent with their reported 198 ± 10 Ma whole rock K–Ar age (Zhang and Zheng 1994). Their major and trace element compositions are consistent with subduction origins and their location along the south or southwest side of the Jinshajiang suture or Litang suture in the central-eastern Qiantang terrane (Fig. 1a) is widely accepted as evidence for subduction southward during the Triassic (Dewey et al. 1988; Pearce and Mei 1988; Hsü et al. 1995; Yin and Harrison 2000; Pan and Ding 2004).

Volcanic rocks that outcrop on and around the Kaixin Ridge to the south of Tuotuohe (Fig. 1b) were previously considered to be entirely Late Permian in age, based on the observation that some occurrences conformably overlie Permian sedimentary rocks and others are overlain by coal-bearing sedimentary rocks inferred to be part of a fossiliferous Permian sequence of the same area (Leeder

et al. 1988; Pearce and Mei 1988). Paleontological data (Sha 1998), however, suggests that both late Permian (*Netschajewia jiangsuensis-polygrina subtilost riata-conveximarginatus assemblages*) and Triassic (*Aulotortus bulbus-A. gaschi (foraminifer) assemblages*) fauna occur in the sedimentary rocks around the Kaixin Ridge.

Subsequent field studies have distinguished both Permian and Triassic volcanic rocks in the Kaixin Ridge area, based on district-wide correlations in flow characteristics. Most fundamentally, Permian volcanic sequences consist entirely of basalts, whereas Triassic sequences are generally composed of basalt-andesite (or rhyolite) suites (Zhang and Zheng 1994; Pan and Ding 2004) (Fig. 1a, b). Geochronological data suggest that most volcanic rocks to the southwest and east of the Kaixin Ridge have Triassic ages [whole rock K–Ar ages of 195 ± 10 to 235 ± 11 Ma: Zhang and Zheng (1994); shown in Fig. 1b]. The volcanic rocks analyzed by Pearce and Mei (1988) are distributed over a section of the 1985 Tibet Geotraverse which extended about 75 km to the north and south of Tuotuohe. The six rocks were compositionally diverse and included picritic basalt, basalt, basaltic andesite, and andesite. A limited number of trace element analyses revealed a mix of subduction-like signatures and Nb-enriched compositions that Pearce and Mei (1988) concluded were consistent with Permian intracontinental rift magmas that had undergone variable extents of crustal assimilation.

Our study area is to the south of Tuotuohe, to the east of the Kaixin Ridge and close to the Qing-Zang highway (Fig. 1b). Field observations suggested that the upper part of the stratigraphy in this area consists mainly of basalts and diabases whereas the lower part contains only minor basalts interlayered with more abundant magnesian andesites. Three samples were selected for age dating in this study, including one of the upper basalts (02TT-8) and examples of the underlying magnesian andesite (02TT-19) and andesite (02TT-20).

Petrography

The Tuotuohe basalts are black, exhibit porphyritic textures, and consist of plagioclase (50–60%), augite (10–35%), magnetite (5–10%), olivine (0–3%) and cryptocrystalline–glassy material (10–15%), and secondary carbonate (2–10%). Phenocrysts are mainly plagioclase, augite and magnetite. Plagioclases (phenocryst and matrix) are generally lath-shaped and some grains or parts were altered into fine sericite. Augites are commonly columnar and some grains or parts were altered to fine chlorite. Olivines were commonly altered into serpentine or chlorite, leaving olivine pseudomorphs. Cryptocrystalline material and some magnetite occur among fine

plagioclases in the matrix. Pore spaces and cavities are generally filled with secondary carbonates. The Tuotuohe diabases are also generally black, exhibit porphyritic texture, and consist of plagioclase (35–45%), augite (50–60%), magnetite (5–10%), and minor olivine (0–2%). Augite and magnetite are mainly xenomorphic and are circled by automorphic (lath-shaped) plagioclases. Some plagioclases are altered into fine sericite and some augites are altered to fine chlorite. The Tuotuohe magnesian andesites are deep grey and exhibit porphyritic texture. They comprise plagioclase (50–60%), augite (2–5%), quartz (1–2%), magnetite (1–2%) and some cryptocrystalline–glassy material (20–35%). Phenocrysts consist of plagioclase and minor augite. Matrices exhibit a microcrystalline–cryptocrystalline texture, and are composed of microcrystals (plagioclase, pyroxene and magnetite) and cryptocrystalline–glassy material. The Tuotuohe andesites are grey and exhibit porphyritic texture, similar to above andesites. But they have different mineral contents: plagioclase (50–60%), hornblende (1–5%), quartz (1–5%), magnetite (1–2%) and some cryptocrystalline–glassy material (25–40%). Phenocrysts mainly consist of plagioclase. Matrices exhibit microcrystalline–cryptocrystalline texture, and are composed of microcrystals (plagioclase, hornblende, magnetite and quartz) and some cryptocrystalline material.

Methods

Samples were initially examined by optical microscopy; unaltered or the least-altered samples were selected for further analysis.

Samples for major and trace element analysis were first split into small chips and leached in 4N hydrochloric acid for 1 h to remove secondary carbonate minerals, then powdered after rinsing with deionized water and drying. Major element oxides (wt%) of most samples except sample 02TT20-1 in this study were analyzed at the Hubei Institute of Geology and Mineral Resources by wavelength dispersive X-ray fluorescence spectrometry. Analytical errors are less than 2%. FeO contents of the samples were determined by conventional wet chemical titration methods. The analytical procedures for FeO and other major elements are described in detail by Gao et al. (1995). Major element oxides (wt%) of Sample 02TT20-1 were determined using a Varian Vista PRO ICP-AES at the Guangzhou Institute of Geochemistry, Chinese Academy of Sciences. The details of the analytical procedures were described by Li et al. (2002). Trace elements, including the rare earth elements (REE), were analyzed using a Perkin-Elmer ELAN 6000 inductively-coupled plasma source mass spectrometer (ICP-MS) at

China University of Geosciences (Wuhan) following procedures described by Hu et al. (2000) and Wang et al. (2007a). The analytical precision for most elements is better than 10%. Nd isotopic compositions were determined using a Finnigan MAT-262 mass spectrometer operated in a static multi-collector mode at the Institute of Geology and Geophysics, Chinese Academy of Sciences, Beijing, following the procedures of Zhang et al. (2002). The $^{143}\text{Nd}/^{144}\text{Nd}$ ratio of the La Jolla standard measured during the period of analysis was $^{143}\text{Nd}/^{144}\text{Nd} = 0.511838 \pm 8$ ($2\sigma_m$). Procedural blanks were about 50 pg for Sm and Nd. The measured $^{143}\text{Nd}/^{144}\text{Nd}$ ratios were normalized to $^{146}\text{Nd}/^{144}\text{Nd} = 0.7219$. Results from major and trace element analyses, along with Nd isotope data, are listed in Table 1.

A sample for sensitive high-resolution ion microprobe (SHRIMP-II) zircon U–Pb dating was collected from the Tuotuohe basalt (sample 02TT-8). Zircon grains were separated using conventional heavy liquid and magnetic techniques. Representative zircon grains were handpicked and mounted in an epoxy resin disc, and then polished and coated with gold film. Internal morphology was examined using both backscatter electron and cathodoluminescence images prior to U–Pb isotopic analyses. The U–Pb isotopic analyses were performed using SHRIMP-II at the Chinese Academy of Geological Science (Beijing). Details of the analytical procedures used for zircon analysis are given by Jian et al. (2003). Inter-element fractionation in ion emission of zircon was corrected relative to the TEMORA reference standard (417 Ma). The uncertainties in ages listed in Table 2 are cited as 1σ , and the weighted mean ages are quoted at 95% confidence level.

Two relatively fresh samples (02TT-19 and 02TT-20) were selected for K–Ar and ^{40}Ar – ^{39}Ar age determination, utilizing MM-1200 and GV-5400 mass spectrometers, respectively, at the Guangzhou Institute of Geochemistry, Chinese Academy of Sciences. The whole rock chips of 30–60 meshes in size were ultrasonically cleaned in distilled water with $< 1\%$ HNO_3 and deionized water, successively, and then dried and handpicked to remove visible contamination. The rock chips of both 02TT-19 and 02TT-20 were then used for K–Ar dating. The K–Ar age data are listed in Table 3. The rock chips of sample 02TT-19 were also used for ^{40}Ar – ^{39}Ar dating. The sample and a monitor standard DRA1 sanidine (Wijbrans et al 1995) with an age of 25.26 ± 0.07 Ma were irradiated in the 49-2 reactor in Beijing for 54 h. Details of the analytical procedures used for ^{40}Ar – ^{39}Ar analysis are given by Qiu (2006) and Qiu and Jiang (2007). The ^{40}Ar – ^{39}Ar dating results are calculated and plotted using the ArArCALC software of Koppers (2002). The ^{40}Ar – ^{39}Ar age data are listed in Table 4.

Table 1 Major oxides (%), trace elemental (ppm) and Nd isotopic compositions of the Nb-enriched basaltic rocks (basalts and diabases)-magnesian andesites-adakites in the Tuotuohe area of the central Qiangtang (Tibet)

No. Sample Rocks	1 02TT-1 Diabase	2 02TT-2 Basalt	3 02TT-3 Diabase	4 02TT-5 Biabase	5 02TT-6 Diabase	6 02TT-6-1 Diabase	7 02TT-7 Basalt	8 02TT-8 Basalt	9 02TT-9 Diabase	10 02TT-10 Basalt
SiO ₂	47.64	46.49	48.64	47.80	48.05	47.78	51.56	47.92	50.30	50.75
TiO ₂	1.82	1.58	1.61	1.80	1.39	1.81	1.56	1.43	1.63	1.47
Al ₂ O ₃	16.15	15.75	16.06	16.47	16.79	16.44	15.79	17.53	16.52	16.67
Fe ₂ O ₃	4.49	3.39	4.44	3.87	4.28	3.76	8.46	8.34	4.77	4.53
FeO	6.05	7.10	6.05	6.70	4.98	6.85	2.78	1.65	4.15	4.58
MnO	0.17	0.17	0.15	0.17	0.14	0.18	0.13	0.11	0.15	0.13
MgO	7.04	8.62	7.56	7.41	8.11	7.47	6.55	6.29	6.69	7.70
CaO	8.44	8.01	6.02	7.41	7.82	7.30	2.91	7.20	9.07	5.18
Na ₂ O	3.77	3.90	4.57	3.90	3.96	3.96	6.68	4.90	3.49	5.72
K ₂ O	0.48	0.07	0.58	0.44	0.59	0.48	0.06	0.09	0.38	0.11
P ₂ O ₅	0.19	0.17	0.16	0.16	0.21	0.16	0.19	0.14	0.19	0.18
LOI	2.62	4.00	3.48	2.80	2.96	2.94	2.90	4.02	2.36	3.36
∑	98.86	99.25	99.32	98.93	99.28	99.13	99.57	99.62	99.70	100.38
Na ₂ O/K ₂ O	8	56	8	8	7	8	111	54	9	52
Mg [#]	0.55	0.60	0.57	0.56	0.62	0.57	0.53	0.55	0.59	0.61
Sc	30.8	30.2	27.7	32.7	28.1	32.5	29.7	26.9	34.2	31.2
V	246	223	218	261	213	258	185	233	255	240
Co	38.1	36.3	37.3	41.3	37.3	40.5	34.6	35.5	36.2	36.1
Ni	114	107	137	133	112	129	118	117	121	154
Rb	8.57	1.66	11.6	9.30	10.9	11.0	1.16	2.51	6.99	2.22
Sr	344	494	717	456	617	455	487	387	458	838
Y	28.1	24.3	26.4	28.4	20.3	28.5	20.7	17.2	23.8	22.6
Zr	156	118	148	168	130	164	157	138	143	136
Nb	8.94	7.29	8.45	9.56	11.7	9.27	13.6	12.5	11.3	10.3
Ba	217	63.4	333	229	397	252	61.4	48.8	249	121
Hf	3.51	2.72	3.25	3.63	2.97	3.54	3.52	2.97	3.19	3.04
Ta	0.63	0.51	0.59	0.64	0.79	0.68	0.95	0.81	0.76	0.68
Pb	10.8	3.21	11.0	6.12	11.1	5.31	13.7	14.0	8.70	10.1
Th	0.95	0.79	0.83	0.83	1.20	0.84	1.28	1.03	1.09	0.97
U	0.35	0.24	0.27	0.32	0.36	0.30	0.41	0.37	0.27	0.36
La	8.46	7.63	8.27	8.22	12.0	7.64	14.3	12.5	10.5	9.04
Ce	21.0	18.4	20.5	20.2	27.3	19.6	31.0	26.9	25.4	22.9
Pr	2.98	2.64	2.82	2.87	3.47	2.81	3.92	3.39	3.36	3.12
Nd	14.4	12.8	13.4	14.1	15.5	13.3	17.3	14.6	15.7	14.3
Sm	3.79	3.42	3.50	3.80	3.47	3.65	3.65	3.06	3.77	3.39
Eu	1.33	1.17	1.32	1.36	1.36	1.36	1.16	1.00	1.41	1.19
Gd	4.31	3.74	4.01	4.37	3.62	4.35	3.53	2.93	4.07	3.69
Tb	0.689	0.608	0.620	0.673	0.563	0.685	0.610	0.496	0.637	0.610
Dy	4.51	3.83	3.97	4.25	3.41	4.41	3.64	2.96	3.95	3.67
Ho	1.07	0.94	0.98	1.08	0.74	1.03	0.82	0.63	0.90	0.80
Er	2.84	2.50	2.68	2.87	2.15	2.91	2.24	1.86	2.50	2.37
Tm	0.42	0.35	0.40	0.41	0.28	0.41	0.29	0.24	0.33	0.31
Yb	2.93	2.51	2.72	2.96	2.06	2.86	2.12	1.75	2.40	2.19
Lu	0.46	0.40	0.44	0.48	0.33	0.49	0.34	0.28	0.37	0.36
Sr/Y	12	20	27	16	30	16	24	23	19	37
La/Yb	3	3	3	3	6	3	7	7	4	4

Table 1 continued

No.	1	2	3	4	5	6	7	8	9	10
Sample	02TT-1	02TT-2	02TT-3	02TT-5	02TT-6	02TT-6-1	02TT-7	02TT-8	02TT-9	02TT-10
Rocks	Diabase	Basalt	Diabase	Biabase	Diabase	Diabase	Basalt	Basalt	Diabase	Basalt
Nb/La	1.1	1.0	1.0	1.2	1.0	1.2	1.0	1.0	1.1	1.1
Nb/U	25.5	30.4	31.3	29.9	32.5	30.9	33.2	33.8	41.9	28.6
Ce/Pb	1.94	5.73	1.86	3.30	2.46	3.69	2.26	1.92	2.92	2.27
Eu/Eu*	1.0	1.0	1.1	1.0	1.2	1.0	1.0	1.0	1.1	1.0
¹⁴⁷ Sm/ ¹⁴⁴ Nd	0.1604	0.1630			0.1358		0.1288		0.1464	
¹⁴³ Nd/ ¹⁴⁴ Nd	0.512848	0.512852			0.512723		0.512668		0.512799	
2σ _m	±14	±15			±12		±14		±13	
(¹⁴³ Nd/ ¹⁴⁴ Nd) ₁	0.512608	0.512608			0.512519		0.512475		0.512578	
εND (t)	5.2	5.2			3.4		2.6		4.6	
εND (0)	4.1	4.2			1.7		0.59		3.1	
T _{DM} (Ga)	0.86	0.90			0.84		0.87		0.80	
No.	11	12	13	14	15	16	17	International standard		
Sample	02TT-11	02TT-12	02TT-19	Qy59	02TT-20	02TT20-1	Qy77B	BHVO-2	BHVO-2(RV)	
Rocks	Basalt	Basalt	MA	MA	Adakite	Adakite	Adakite			
SiO ₂	49.22	48.82	61.39	62.86	62.39	61.47	59.38			
TiO ₂	1.45	1.47	0.61	0.54	0.59	0.63	0.66			
Al ₂ O ₃	17.19	16.67	15.34	16.76	16.03	17.57	18.28			
Fe ₂ O ₃	7.60	4.25	5.29	5.19	4.22	6.29	4.95			
FeO	2.42	5.38	2.70		2.32					
MnO	0.11	0.16	0.12	0.20	0.11	0.10	0.12			
MgO	5.80	8.06	4.15	5.00	3.50	2.84	1.70			
CaO	6.43	5.64	1.30	3.70	1.88	2.76	2.30			
Na ₂ O	5.70	4.97	5.73	4.54	5.94	6.45	8.70			
K ₂ O	0.03	0.25	0.23	0.19	0.19	0.14	0.75			
P ₂ O ₅	0.23	0.21	0.03	0.12	0.03	0.01	0.38			
LOI	3.40	3.32	2.58	1.00	2.28	2.20	1.82			
Σ	99.58	99.20	99.47	100.10	99.48	100.45	99.04			
Na ₂ O/K ₂ O	190	20	25	24	31	49	12			
Mg [#]	0.53	0.61	0.50	0.66	0.50	0.47	0.40			
Sc	21.6	26.5	18.1	23.9	18.9	19.7	13.6	32.0	32.0	
V	196	226	145	NA	142	159	NA	316	317	
Co	31.2	36.3	20.9	NA	16.7	13.8	NA	44.6	45.0	
Ni	112	128	22.6	NA	18.5	16.92	NA	129	119	
Rb	0.67	5.58	4.98	4	3.73	2.49	NA	9.34	9.8	
Sr	501	1392	220	498	310	498	NA	392	389	
Y	15.6	20.3	8.75	11	9.32	11.1	NA	26.7	26.0	
Zr	120	140	92.6	109	94.0	95.7	129	170	172	
Nb	13.5	14.1	2.52	11	3.36	2.57	8	18.4	18.0	
Ba	36.0	277	73.1	NA	50.0	35.8	NA	126	130	
Hf	2.67	2.96	2.22	2.91	2.33	2.48	3.46	4.40	4.10	
Ta	0.85	0.95	0.169	0.74	0.189	0.182	0.49	1.34	1.40	
Pb	8.96	10.4	4.83		4.06	9.41		1.76	2.60	
Th	1.18	1.17	1.65	4.1	1.71	1.82	6	1.23	1.20	
U	0.41	0.36	0.586	NA	0.745	0.834	NA	0.43	0.42	
La	13.1	12.8	18.8	14	25.1	42.5	42	14.4	15.0	
Ce	29.4	29.9	27.0	25.5	34.4	54.6	69.2	35.8	38.0	
Pr	3.78	3.94	2.64	NA	3.37	5.04	NA	5.03	5.70	

Table 1 continued

No.	11	12	13	14	15	16	17	International standard	
Sample	02TT-11	02TT-12	02TT-19	Qy59	02TT-20	02TT20-1	Qy77B	BHVO-2	BHVO-2(RV)
Rocks	Basalt	Basalt	MA	MA	Adakite	Adakite	Adakite		
Nd	15.9	17.3	8.94	12.9	11.4	17.1	27	25.1	25.0
Sm	3.14	3.73	1.37	2.8	1.80	2.60	5	6.06	6.20
Eu	1.04	1.33	0.522	0.79	0.773	1.25	1.37	1.98	2.06
Gd	3.04	4.07	1.18	NA	1.61	2.32	NA	6.03	6.30
Tb	0.482	0.600	0.202	0.45	0.268	0.355	0.6	0.88	0.90
Dy	2.73	3.56	1.18	NA	1.49	1.97	NA	5.11	5.20
Ho	0.58	0.75	0.267	NA	0.301	0.375	NA	1.01	1.04
Er	1.76	2.24	0.827	NA	0.879	1.02	NA	2.58	2.40
Tm	0.22	0.27	0.134	NA	0.144	0.154	NA	0.34	0.33
Yb	1.59	2.00	0.974	1.00	0.913	1.03	1.0	2.12	2.00
Lu	0.26	0.33	0.163	0.15	0.151	0.158	0.17	0.3	0.28
Sr/Y	32	69	25	45	33	45			
La/Yb	8	6	19	14	27	41	42		
Nb/La	1.0	1.1	0.1	0.8	0.1	0.1	0.2		
Nb/U	32.9	39.2	4.3		4.5	3.1			
Ce/Pb	3.28	2.88	5.59		8.47	5.80			
Eu/Eu*	1.0	1.0	1.3		1.4	1.6			
¹⁴⁷ Sm/ ¹⁴⁴ Nd	0.1198		0.0931		0.0959	0.0926			
¹⁴³ Nd/ ¹⁴⁴ Nd	0.512675		0.512527		0.512549	0.512533			
2σ _m	±12		±12		±9	±13			
(¹⁴³ Nd/ ¹⁴⁴ Nd) _i	0.512494		0.512387		0.512405	0.512394			
ε _{ND} (t)	3.0		0.86		1.2	0.99			
ε _{ND} (0)	0.72		-2.2		-1.7	-2.0			
T _{DM}	0.77		0.79		0.78	0.78			

MA Magnesian andesite. No. 1–13, 15 and 16 are from this study, and No. 14 and 17 are after Pearce and Mei (1988). RV Recommended values. $Eu/Eu^* = (Eu/0.07035)/((Sm/0.195)*(Gd/0.259))^{1/2}$

Analytical results

Geochemistry

The basalts have silica contents between 46.49 and 51.56 wt%, MgO contents between 5.80 and 8.62 wt% (Fig. 2a) and Mg[#] ($Mg^{2+}/(Fe^{2+} + Mg^{2+})$) between 0.53 and 0.62. They are highly sodic ($Na_2O/K_2O > 7$) and Ti-rich ($TiO_2 = 1.43$ – 1.82 wt%). Their trace element contents differ from the vast majority of arc basalts in terms of higher contents of Nb (7.3–14.1 ppm), Ta (0.51–0.95 ppm), Zr (118–164 ppm) and elevated Nb/La (1.0–1.2) and Nb/U (26–41) ratios (Fig. 3a, b; Table 1). They also exhibit distinctly lower Ce/Pb and higher Ba/La ratios than MORB and OIB (Fig. 3C). Niobium variation diagrams for the basalts define positive correlations with other incompatible elements, such as Th and La (Fig. 4a, b), but are negatively correlated with Y, Yb, and ε_{ND} (t), and poorly correlated with Rb (Fig. 4c–f). The basalts have lower Nb/U ratios than typical OIB, N-MORB and

E-MORB (Fig. 3a; Sun and McDonough 1989) and display pronounced positive anomalies in Ba, Sr and Zr that are rare in these rock types (Fig. 5a). Their REE spectra are steeper than is typical of E-MORB but less fractionated than OIB patterns (Fig. 5a). However, the Tuotuohe basalts have incompatible trace element contents similar to those of Nb-enriched basalts (NEB) reported from the Philippines and Mexico (Sajona et al. 1993; Aguillón-Robles et al. 2001). The mantle-normalised Nb/La ratios of the Tuotuohe basalts exceed the 0.5 value used to define NEB (Sajona et al. 1996) and they are referred to as NEB below for ease of discussion. Although the term does not necessarily carry a genetic connotation, we argue below that the Tuotuohe basalts do in fact have an arc-related origin.

The two magnesian andesites have SiO₂ contents of 61.39 and 62.86 wt%, exhibit high MgO (4.15 and 5.00 wt%) and Mg[#] (0.50 and 0.66), and are similar to typical magnesian andesites (Polat and Kerrich 2002). They have low Yb (<1.0) and Y (<11 ppm) contents, high Al₂O₃ (15.34 and 16.76 wt%) contents and high Na₂O/K₂O (24–

Table 2 SHRIMP U–Pb isotopic data for zircons from the basalt in the Tuotuohe area of the central Qiangtang block (Tibet)

Analysis #	²⁰⁶ Pbc (%)	U ppm	Th ppm	²³² Th/ ²³⁸ U	²⁰⁶ Pb* (10 ⁻⁶)	²⁰⁶ Pb/ ²³⁸ U (age, Ma)	²⁰⁷ Pb*/ ²⁰⁶ Pb* ±%	²⁰⁷ Pb*/ ²³⁵ U ±%	²⁰⁶ Pb*/ ²³⁸ U ± (%)			
1	0.57	478	159	0.34	15.6	238.2 ± 7.0	0.0547	4.7	0.284	5.6	0.0376	3.0
2	0.58	289	85	0.31	15.5	388 ± 12	0.0597	4.9	0.510	5.8	0.0620	3.1
3	0.46	842	361	0.44	26.4	230.3 ± 6.6	0.0533	3.3	0.268	4.4	0.0364	2.9
4	0.42	472	256	0.56	28.1	431 ± 12	0.0590	2.7	0.563	4.0	0.0691	2.9
5	0.19	568	193	0.35	17.3	223.8 ± 6.5	0.0538	3.9	0.262	4.9	0.0353	3.0
6	0.11	1331	317	0.25	60.1	329.9 ± 9.2	0.0539	3.8	0.390	4.8	0.0525	2.8
7	0.43	69	45	0.67	7.33	749 ± 24	0.0839	5.1	1.426	6.1	0.1233	3.5
8	0.61	944	632	0.69	28.1	218 ± 13	0.0506	3.4	0.240	6.9	0.0345	6.0
9	0.00	207	13	0.07	27.7	933 ± 26	0.0760	1.8	1.631	3.5	0.1557	3.0
10	0.41	155	189	1.26	18.4	830 ± 4.4	0.0721	2.7	1.366	4.2	0.1374	3.2
11	0.04	252	98	0.40	117	2,782 ± 68	0.1872	2.6	13.93	4.0	0.5400	3.0
12	0.07	1384	417	0.31	62.9	332.2 ± 9.2	0.05392	1.8	0.393	3.4	0.0529	2.8
13	0.20	337	140	0.43	62.5	1,258 ± 34	0.0933	2.9	2.77	4.1	0.2154	2.9
14	0.46	323	151	0.48	20.0	446 ± 13	0.0607	3.0	0.600	4.2	0.0716	3.0
15	0.00	711	106	0.15	104	1,013 ± 27	0.07683	1.2	1.803	3.1	0.1702	2.9
16	0.87	36	15	0.42	4.04	784 ± 31	0.0822	7.9	1.47	8.9	0.1293	4.1
17	0.15	2378	881	0.38	108	332.5 ± 9.2	0.06095	1.3	0.445	3.1	0.0529	2.8

Errors are 1-sigma; Pb_c and Pb* indicate the common and radiogenic portions, respectively. Error in standard calibration was 0.50% (not included in above errors but required when comparing data from different mounts). Common Pb corrected using measured ²⁰⁴Pb

Table 3 K–Ar ages on whole rock powders

Sample	Rock	Weight (g)	K (%)	⁴⁰ Ar total 10 ⁻¹¹ (mol/g)	⁴⁰ Ar radiogenic 10 ⁻¹¹ (mol/g)	⁴⁰ K 10 ⁻⁹ (mol/g)	Age (± 2σ) (Ma)
02TT-19	Magnesian andesite	0.1465	0.194	1.080	8.493	5.790	236.3 ± 3.8
02TT-20	Adakite	0.107	0.149	8.829	6.053	4.447	220.2 ± 3.4

Parameters for ⁴⁰K: λ_e = 0.581 × 10⁻¹⁰ year⁻¹; λ_β = 4.962 × 10⁻¹⁰ year⁻¹; ⁴⁰K = 0.01167 atom%

25) ratios (Table 1), and weak positive Eu but strong negative Nb and Ta anomalies (Fig. 5b), similar to local adakites. They have variable Sr contents (220 and 498 ppm) and Sr/Y ratios (25 and 45), relatively low La/Yb ratios (14 and 19) and slightly positive Ti anomalies (Fig. 5b).

The Tuotuohe andesites are characterized by intermediate compositions (SiO₂ = 59.38–62.39 wt%), high Al₂O₃ (16.03–18.28 wt%), Na₂O (5.94–8.70 wt%) and Sr (310–498 ppm) contents, distinctly positive Eu anomalies, and low heavy rare earth element contents (REE) (Yb < 1.03 ppm), and low Y contents (<11.1 ppm), which result in high Na₂O/K₂O (12–49), Sr/Y (33–45) and La/Yb (27–42) ratios (Table 1) that are diagnostic features of adakitic lavas in subduction-zone settings (Fig. 6a) (Defant and Drummond 1990; Kay et al. 1993; Martin 1999). The adakites and magnesian andesites can be considered as the low- and high-Mg parts of a single compositional group (Fig. 2). Their multi-element patterns are directly comparable (Fig. 5b) and show strongly fractionated REE spectra,

negative Nb, Ta and Ti anomalies, negligible to slightly positive Sr anomalies with respect to adjacent elements and very low Ba and Rb contents (Fig. 5b). The adakites and magnesian andesites also display similar ε_{ND}(t) (+0.86 to +1.21) but their isotopic compositions are distinct from the NEB, which have higher and more variable ε_{ND}(t) (+2.57 to +5.16, Table 1).

Geochronological data

Results from SHRIMP-II zircon U–Pb analyses are listed in Table 2 and Fig. 7. Zircons were extracted from one ~1 kg NEB flow sample (02TT-8) and yield a wide range of ages (Table 2; Fig. 7). The cluster of ~750–1,000 Ma zircon ages corresponds to the most prominent cluster of ages reported from late Triassic Qiangtang sandstones of the Shuanghu area at the eastern end of the blueschist-bearing metamorphic belt (Fig. 1a). The

Table 4 Argon isotope analyses for the magnesian andesite (sample 02TT-19)

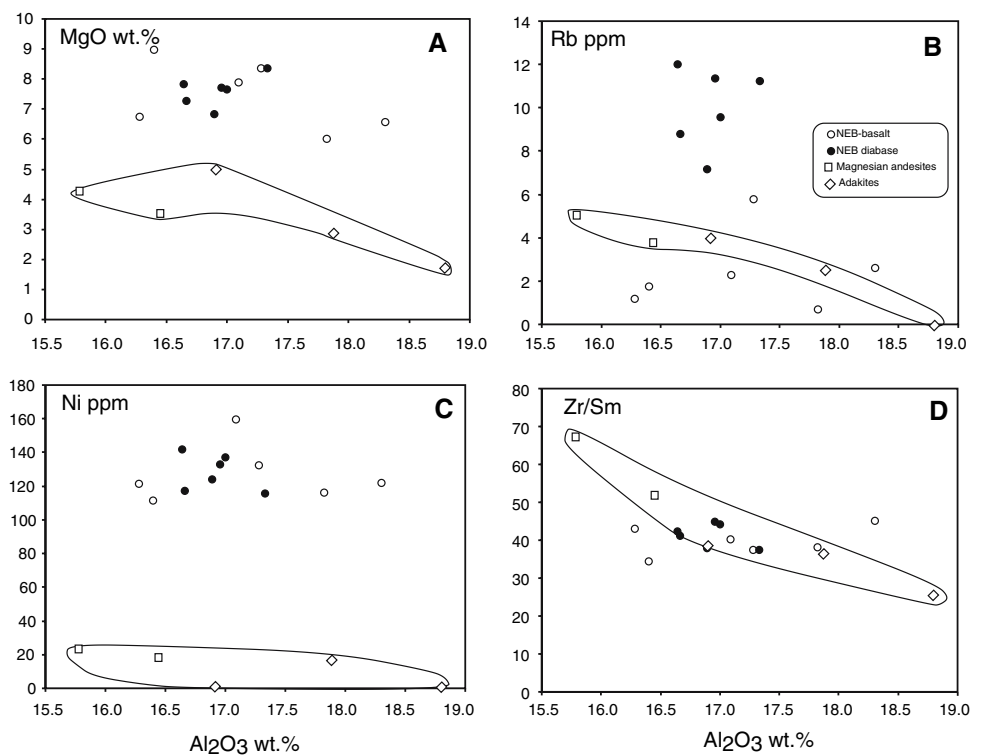
Incremental Heating	$^{36}\text{Ar}(\text{a})$	$^{37}\text{Ar}(\text{ca})$	$^{38}\text{Ar}(\text{cl})$	$^{39}\text{Ar}(\text{k})$	$^{40}\text{Ar}(\text{r})$	$^{40}\text{Ar}(\text{r})(\%)$	$^{39}\text{Ar}(\text{k})(\%)$	Age $\pm 2\sigma(\text{Ma})$
07M2064B 2.0 W	0.000025	0.000406	0.000003	0.000649	0.008247	53.21	5.11	231.53 \pm 6.77
07M2064C 2.5 W	0.000017	0.000254	0.000002	0.000394	0.004119	44.43	3.11	192.42 \pm 14.84
07M2064D 3.0 W	0.000024	0.000362	0.000003	0.000422	0.004036	36.16	3.32	177.08 \pm 9.94
07M2064E 3.5 W	0.000033	0.000461	0.000005	0.000498	0.005467	36.22	3.92	201.76 \pm 10.19
07M2064F 4.0 W	0.000034	0.000743	0.000007	0.000601	0.006687	40.17	4.74	204.23 \pm 9.16
07M2064H 4.5 W	0.000036	0.001163	0.000005	0.000570	0.005832	35.52	4.49	188.58 \pm 10.63
07M2064I 5.0 W	0.000035	0.000908	0.000007	0.000671	0.007732	42.68	5.28	211.26 \pm 8.47
07M2064J 5.7 W	0.000037	0.001159	0.000009	0.000848	0.009819	47.26	6.68	212.22 \pm 7.46
07M2064K 6.4 W	0.000039	0.000949	0.000008	0.000968	0.011151	49.31	7.62	211.22 \pm 5.98
07M2064L 7.2 W	0.000040	0.000889	0.000009	0.000824	0.009364	44.26	6.49	208.55 \pm 7.55
07M2064N 8.2 W	0.000029	0.000829	0.000007	0.000825	0.009908	53.46	6.50	219.61 \pm 6.13
07M2064O 9.5 W	0.000042	0.001927	0.000012	0.001119	0.013898	53.02	8.81	226.70 \pm 4.34
07M2064P 11.5 W	0.000029	0.000992	0.000008	0.000766	0.009263	51.90	6.04	220.95 \pm 5.80
07M2064Q 15.0 W	0.000047	0.002000	0.000014	0.001250	0.015293	52.42	9.85	223.50 \pm 5.34
07M2064R 20.0 W	0.000027	0.000574	0.000007	0.000766	0.007972	49.65	6.04	191.76 \pm 6.86
07M2064S 30.0 W	0.000050	0.001428	0.000013	0.001522	0.017528	54.23	11.99	211.12 \pm 4.36

$J = 0.0107774 \pm 0.0000162$, $T_{\text{p(weighted plateau)}} = 219.0 \pm 5.0$, $T_{\text{f(total fusion)}} = 211.3 \pm 1.9$, $T_{\text{n(normal isochron)}} = 252.0 \pm 29.7$, $T_{\text{i(inverse isochron)}} = 247.6 \pm 54.0$

oldest xenocrystic zircon age ($\sim 2,800$ Ma) also lies within the range reported from these sedimentary rocks (Fig. 9; Kapp et al. 2003). The absence of 1,600–2,000 Ma ages is also consistent with the low abundance of zircons with these ages in the Shuanghu sedimentary

rocks. The NEB zircon age distribution, however, contrasts with that of the Triassic Songpan-Ganzi flysch complex located north of the Qiangtang terrane, which is dominated by 1,600–2,000 Ma zircons (Bruguier et al. 1997).

Fig. 2 Alumina variation diagrams for Tuotuohe rock types. The magnesian andesites and adakites define continuous compositional trends. Parental magmas to the Nb-enriched basalt flows and fine-grained diabase intrusions have undergone differing degrees of crystal fractionation



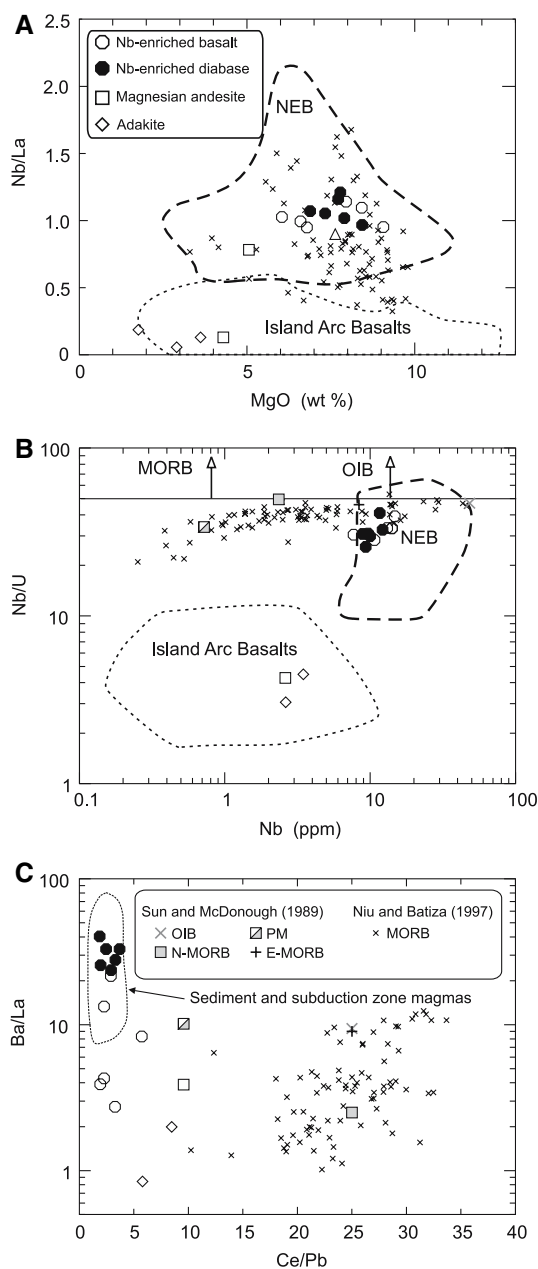


Fig. 3 **a** Nb/La versus MgO (wt%) diagram [after Kepezhinskas et al. (1996)]. **b** Nb/U versus Nb diagram [after Kepezhinskas et al. (1996)]. MORB and OIB fields are after Hofmann (1986) and Hofmann et al. (1986). **c** Ba/La versus Ce/Pb diagram [after Haase et al. (1996)]. The fields of the island arc basalts and NEB (Nb-enriched basalts) are after Kepezhinskas et al. (1996). The field of sediment and subduction zone magmas is after Haase et al. (1996). The data for MORB (middle oceanic ridge basalts) or N (or E)-MORB, OIB (oceanic island basalts) and PM (primitive mantle) are from Sun and McDonough (1989) and Niu and Batiza (1997)

The four youngest age results obtained from two zircons with magmatic oscillatory zonings and high Th/U ratios (0.33–0.67) define a concordant age with a weighted mean $^{206}\text{Pb}/^{238}\text{U}$ age of 229 ± 7 Ma (2σ) (MSWD = 1.01, Table 2, Fig. 7), indicating that the Tuotuohe NEB are not

Permian in age and are likely to be Triassic in age as inferred by Pan and Ding (2004) and Zhang and Zheng (1994).

The magnesian andesite (02TT-19) and adakite (02TT-20) in this study give 236.3 ± 3.8 Ma and 220.2 ± 3.4 Ma K–Ar ages, respectively (Table 3), which are interpreted to be their Triassic eruption ages. Additionally, ^{40}Ar – ^{39}Ar age data for Sample 02TT-19 are plotted in Fig. 8. It yielded plateau and inverse isochron ages of 219.0 ± 5.0 Ma and 247.6 ± 54.0 Ma, respectively. Collectively, the new geochronological data (219–236 Ma) are consistent, within errors, with observed local field relations, the Triassic K–Ar ages (213–235 Ma) obtained by Zhang and Zheng (1994) for volcanic rocks to the south and east of Tuotuohe (Fig. 1b), and fossil evidence for Triassic strata in the area (Sha 1998).

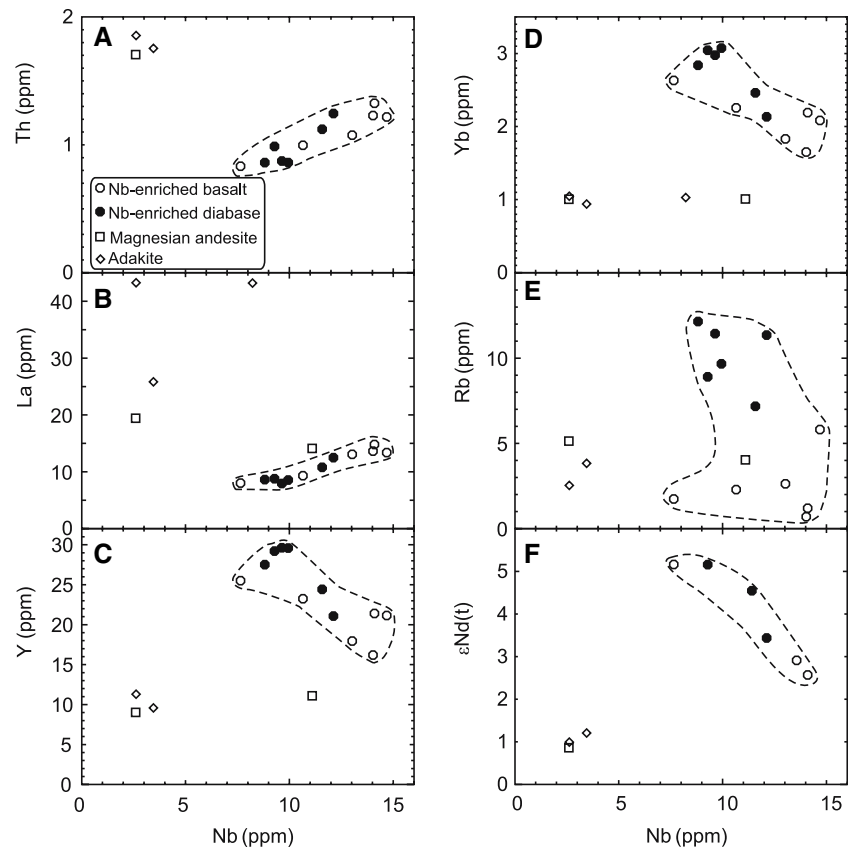
Discussion

Stratigraphic correlations in the Central Qiangtang Belt

The new geochronological results have important implications for the tectonic models applied to the central Qiangtang belt. The age data suggest that the Tuotuohe volcanic rocks assigned to Permian rifting by Pearce and Mei (1988) are actually the same age as Triassic basalt-andesite outcrops located 30 km to the north and eastward (the Batang Group), and likely formed in the same subduction-related geodynamic environment.

Kapp et al. (2003) account for the age distribution of inherited zircons in metasedimentary rocks from Shuanghu in terms of regional-scale sources, such as the South China Block (800–1,200 Ma zircons). Accordingly, they consider that their results provide a “preliminary detrital zircon fingerprint for Qiangtang metasedimentary rocks” (p. 17–17). The fact that a similar zircon age distribution (Fig. 9) was obtained from a small sample of Tuotuohe basalt suggests that the mafic lava may have inherited zircons from similar sedimentary rocks. If so, then zircon entrainment probably occurred either in shallow-level magma chambers, or after eruption, rather than in the deep crust. Either scenario would permit relatively rapid post-eruptive cooling of the magma following inheritance, which would favor preservation of xenocrystic zircon and allow for crystallisation of new groundmass zircons. For example, the zircon crystals are euhedral and display outer oscillatory zoning that truncates inner zones, indicating late stability of zircon in the mafic magma. Hansmann and Oberlie (1991) show that similar zircon occurrences in gabbro and diorite are attributable to relatively short inclusion times for xenocrystic grains in the mafic magmas and crystallisation of new zircon on xenocrystic seeds after the magmas had partially solidified.

Fig. 4 Incompatible elements (Th, La, Y, Yb and Rb) and $\varepsilon_{\text{Nd}}(t)$ versus Nb plots of the Tuotuohe Nb-enriched basalts and diabases, magnesian andesites and adakites. All data are from Table 1



Pearce and Mei (1988) noted that the Batang Group volcanic rocks are underlain by Triassic fluvial conglomerates and sandstones. Based on the findings of Kapp et al. (2003), those sedimentary rocks are likely to provide an inherited zircon age “fingerprint” analogous to that found in the Tuotuohe NEB. Accordingly, the zircon ages documented for the Tuotuohe basalt not only establish a similar eruption age to that of the Batang Group but also suggest that both areas have similar volcano-sedimentary successions.

The origin of Qiangtang adakites and NEB

Compositional similarities between magmas generated by partial melting of the mafic lower crust under eclogite-facies conditions on the one hand, and slab melting on the other, provide two alternative sources for adakitic rocks (e.g., Defant and Drummond 1990; Atherton and Petford 1993; Kay and Kay 1993; Defant and Kepezhinskas 2001; Xu et al. 2002; Gao et al. 2004; Hou et al. 2004; Chung et al. 2005; Zhou et al. 2006; Wang et al. 2005, 2007a, b). In the case of the Tuotuohe adakites, their Triassic age is consistent with slab melting during the southward subduction of the Paleo-Tethyan oceanic lithosphere along the Jinshajiang suture (Dewey et al. 1988; Yin and Harrison 2000; Pan and

Ding 2004). Moreover, their very high Na_2O contents (Table 1) and low Th contents and Th/Ce ratios (Fig. 6b) indicate that their compositions are more consistent with slab melting rather than with magma originating in the lower crust (Zhou et al. 2006; Wang et al. 2007a, b). Empirically, adakites generated in the lower crust tend to be more K-rich and are distinguished by markedly higher contents of strongly incompatible elements such as Rb, Ba, Th, and U (e.g., Wang et al. 2005, 2007a, b).

The compositional gradation between the Tuotuohe adakites and associated magnesian andesites also provides strong support for an adakite origin in the slab. The magnesian magmas are most plausibly accounted for by the variable interaction of adakitic magmas and mantle wedge peridotite, which is inconsistent with a lower crustal source (e.g., Defant and Kepezhinskas 2001; Polat and Kerrich 2002; Rapp et al. 1999).

Isotopic evidence also supports a slab origin for the Tuotuohe adakites. For example, they have Nd isotopic compositions (Table 1) that are distinct from those of Late Triassic syn-collisional crust-derived granites in the Songpan-Ganzi, Kunlun Mountain and Northern Qiangtang terranes (Fig. 10a) (Roger et al. 2003, and references therein). Although their $\varepsilon_{\text{Nd}}(t)$ values are lower than Carboniferous MORB distributed along the Jinshajiang suture (Xu and Castillo 2004), the adakites plot in the field

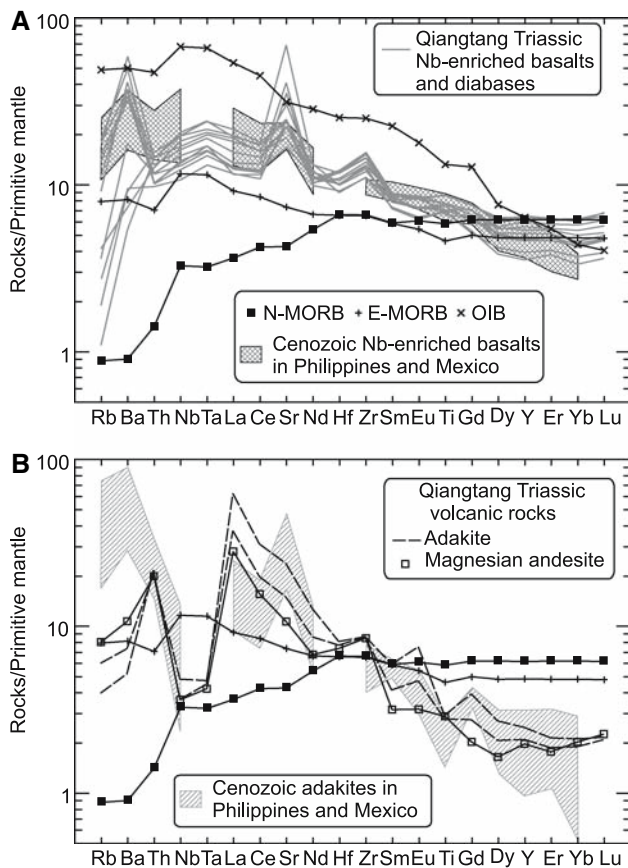


Fig. 5 Primitive mantle-normalized multi-element profiles of Nb-enriched basalts and diabases (**a**) adakites and magnesian andesite (**b**) and in the Tuotuohe area. Primitive mantle normalizing values, N-MORB, E-MORB and OIB data are from Sun and McDonough (1989). Data sources of Cenozoic adakites and Nb-enriched basalts in Philippines and Mexico are from Sajona et al. (1993) and Aguillón-Robles et al. (2001), respectively

of 260–231 Ma basalts located north of the Jinshajiang suture (Fig. 10a), which probably represented newly formed oceanic crust at the time of adakite magmatism (Qu and Hou 2002; Pan and Ding 2004; Song et al. 2004). Collectively, these lines of evidence indicate that the Tuotuohe Middle Triassic adakites were generated by partial melting of subducted oceanic crust that was likely to have been young (≤ 30 Ma) at the time of subduction, based on the known ages of MORB along the Jinshajiang suture.

The xenolithic zircons in the NEB indicate some degree of crustal contamination. However, we suggest that such contamination did not play a significant role in the petrogenesis of NEBs. For example, the range of $\varepsilon_{\text{ND}}(t)$ and T_{DM} defined by the NEB (+2.6 to +5.2 and 0.84–0.90 Ga) is smaller than that defined by MORB along the Jinshajiang suture (+4.3 to +8.2 and 1.06–3.57 Ga; Xu and Castillo 2004). In general, crustal contamination will cause relative Nb-depletion (Dungan et al. 1986) rather than Nb-enrichment in basalts (Fig. 5a). A negative correlation between

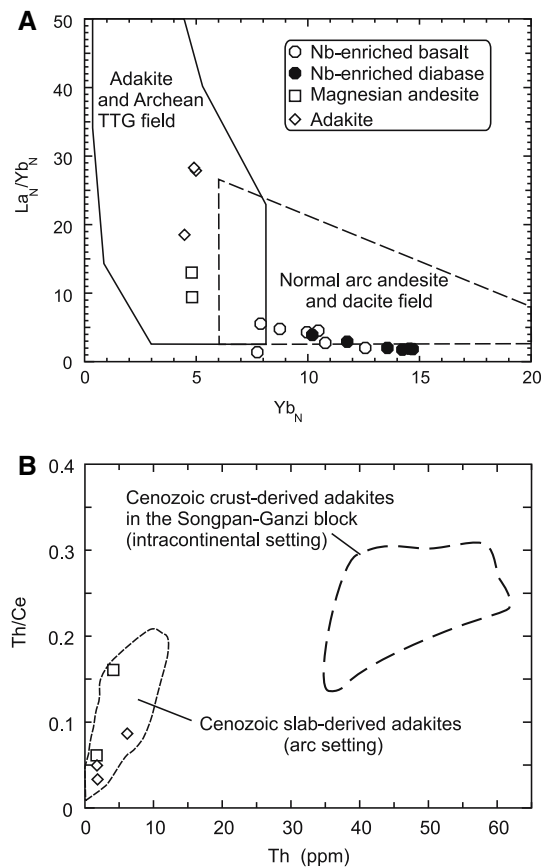


Fig. 6 **a** La_N/Yb_N versus Yb_N diagram for Tuotuohe mafic to intermediate rock types (chondrite-normalised values; Boynton 1984). Adakites and magnesian andesites plot within the field of adakites and Archean TTG. Modified from Martin (1999). **b** Th/Ce versus Th diagram of adakites. Data of Cenozoic crust-derived adakite in the Songpan-Ganzi block (intracontinental setting) are from Wang et al. (2005). Data of Cenozoic slab-derived adakites (arc setting) are from Defant and Drummond (1990), Defant et al. (1992), Kay et al. (1993), Sajona et al. (1993, 1996), Kepezhinskias et al. (1996, 1997), Martin (1999), Aguillón-Robles et al. (2001) and Defant and Kepezhinskias (2001), and references therein

Th/Nb versus La/Sm ratios (Fig. 10c) and no correlation between Th/Nb and $\varepsilon_{\text{ND}}(t)$ values (Fig. 10b) for NEB samples are also not consistent with extensive crustal contamination (e.g., Puchtel et al. 1997; Condie 2003). Their slightly variable $\varepsilon_{\text{ND}}(t)$ values are possibly related to melt metasomatism, however, because the $\varepsilon_{\text{ND}}(t)$ values clearly decrease with increasing Nb contents (Fig. 4f). The lack of significant contamination may be reconciled with the presence of inherited zircons in the NEB if the xenolithic crystals were concentrated in sandstones prior to entrainment in the mafic magmas, as suggested above. Minor assimilation of these sedimentary rocks could then contribute a disproportionately large number of zircons with negligible effect on the major element compositions of the NEB magmas.

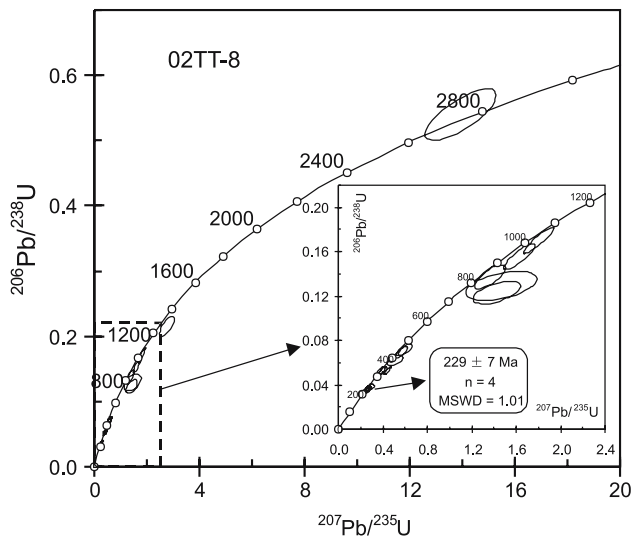


Fig. 7 SHRIMP zircon U–Pb concordia diagram for the Nb-enriched basalt (sample 02TT-8). Four zircons with high Th/U ratios (0.33–0.67) have a concordant age with a weighted mean $^{206}\text{Pb}/^{238}\text{U}$ age of 229 ± 7 Ma (2σ) (MSWD = 1.01), indicating that the volcanic rocks were produced in the Middle Triassic. The age distributions of xenocrystic zircons are similar to Triassic Qiangtang sedimentary rocks (Fig. 9), suggesting that the zircons were inherited at shallow crustal levels shortly before or during eruption

Although Castillo et al. (2002 and references therein) argued that NEBs may result from mixing of an intra-plate style enriched mantle component with a more abundant depleted mantle wedge component, many workers consider them to be derived from a mantle source that was metasomatized by adakitic melts (Defant and Kepezhinskas 2001 and references therein). As noted above, continuous compositional trends (Fig. 2) between the Tuotuohe adakites and magnesian andesites themselves provide evidence for the interaction of slab melts with mantle peridotite. Chemical trends within the NEB suite also serve to constrain the genesis of the basaltic rocks.

The poor correlation between Rb and Nb (or Ta) (Fig. 4e) suggests that the enrichment of Nb and Ta in the Tuotuohe NEBs is not related to either varying degrees of partial melting or source depletion, given that these controls would create positive correlations between Rb and the HFSE. Figure 10d illustrates the differing trends expected for fluid-related enrichment of the mantle and melt-related enrichment. Rubidium is a strongly mobilised element in hydrous fluids, based on its partition coefficients for (Na, K) Cl fluids with andesitic melt (≥ 2.7 –8.0) (Keppler 1996). The Rb/Y ratios of adakites, however, are comparatively low and produce sub-horizontal trends on Rb/Y versus Nb/Y plots (Fig. 10d) defined by slab melt entrapment in the mantle. The variably positive anomalies for Ba, Nb, Ta, Sr, Zr on mantle-normalised plots (Fig. 5a) and positive correlations between Th, La and Nb (Fig. 4a, b) indicate a

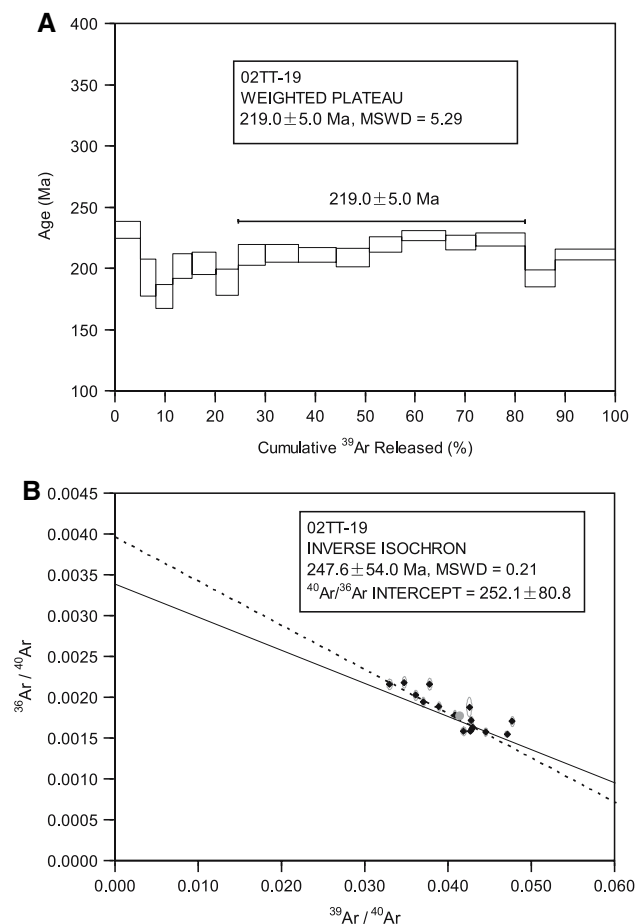


Fig. 8 The $^{40}\text{Ar}/^{39}\text{Ar}$ age spectra diagrams for the magnesian andesite (02TT-19)

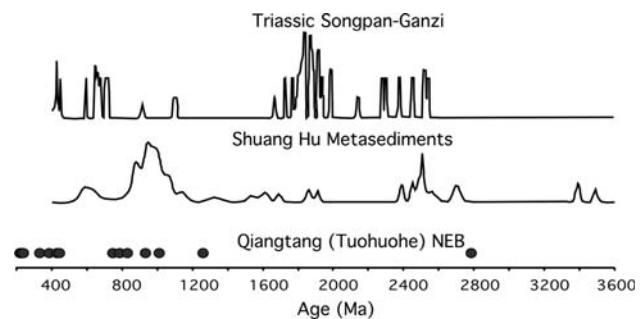


Fig. 9 Correlations and origins of Qiangtang NEB. The age distribution of zircons in Tuotuohe Nb enriched basalt is distinct from the age spectra reported for detrital zircons of Songpan-Ganzi Flysch but resembles that of Triassic Shuanghu sandstones. The Tuotuohe NEB may correlate with the Batang volcanics, which overlie Triassic-aged sandstones and conglomerates. Modified from Kapp et al. (2003)

mantle source metasomatized by igneous melts, which mobilize the HFSE far more readily than aqueous fluids (Keppler 1996). The negative correlations between Y, Yb, $\varepsilon_{\text{ND}}(t)$ and Nb (or Ta) (Fig. 4c, d, f) indicate that this melt was low in Y, Yb and $\varepsilon_{\text{ND}}(t)$, similar to the associated

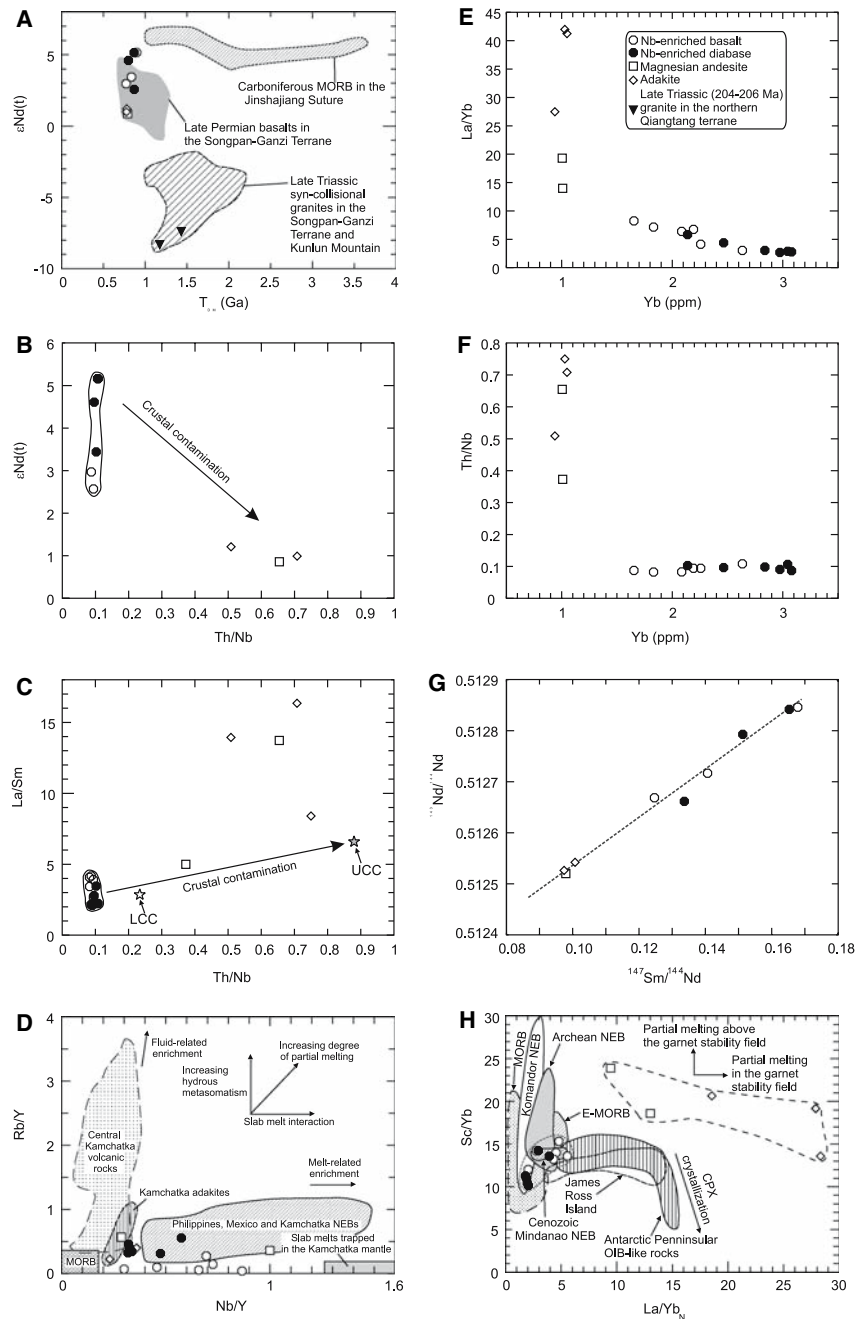


Fig. 10 **a** $\epsilon_{\text{Nd}}(t)$ versus T_{DM} (Ga) diagram of the Tuotuohe Nb-enriched basalts and diabases, magnesian andesites and adakites. $T_{\text{DM}} = 1/\lambda_{\text{Sm}} \ln\{1 + [(^{143}\text{Nd}/^{144}\text{Nd})_{\text{S}} - 0.51315]/[(^{147}\text{Sm}/^{144}\text{Nd})_{\text{S}} - 0.2137]\}$, where S = sample, the decay constant (λ_{Sm}) used in the calculation was 0.00654 Ga^{-1} . Data of Carboniferous MORB in the Jinshajiang Suture, Late Permian basalts in the Songpan-Ganzi Terrane and Late Triassic syn-collisional granites in the Songpan-Ganzi, Kunlun Mountain and northern Qiangtang Terranes are from Xu and Castillo (2004), Song et al. (2004) and Roger et al. (2003), respectively. **b** $\epsilon_{\text{Nd}}(t)$ versus Th/Nb diagram. NEB samples do not exhibit correlation between Th/Nb and $\epsilon_{\text{Nd}}(t)$ values, and their slightly variable $\epsilon_{\text{Nd}}(t)$ values are possibly related to melt metasomatism because the $\epsilon_{\text{Nd}}(t)$ values clearly decrease with the increasing

of Nb contents (Fig. 4f). **c** La/Sm versus Th/Nb diagram. Data for LCC (lower continental crust) and UCC (upper continental crust) are from Rudnick and Gao (2003). **d** Rb/Y versus Nb/Y diagram (after Kepezhinskas et al. (1997)). Data of Philippines, Mexico and Kamchatka magmas are from Sajona et al. (1993), Aguillón-Robles et al. (2001) and Kepezhinskas et al. (1997), respectively. **e** La/Yb versus Yb diagram. **f** Th/Nb versus Yb diagram. **g** $^{143}\text{Nd}/^{144}\text{Nd}$ versus $^{147}\text{Sm}/^{144}\text{Nd}$ diagram of the Tuotuohe Nb-enriched basalts, magnesian andesites and adakites. **h** Sc/Yb versus La/Yb_N plot for Tuotuohe Nb enriched basalts and diabases, magnesian andesites and adakites, modern MORB and E-MORB, Cenozoic NEBs [Mindanao (Sajona et al. 1993) and Komandor (Yogodzinski et al. 1994)] and Archean NEBs (Wyman et al. 2000). Figure adapted from Wyman et al. (2000)

adakites (Table 1). Variable contributions from an intraplate style mantle component, as required in the Castillo et al. (2002) model, can account for some trends in the Tuotuohe data, such as the negative correlation observed on a La/Yb versus Yb plot (Fig. 10e), but is not consistent with the data as a whole. For example, the NEBs do not display the correlation between Th/Nb and Yb (Fig. 10f), or between La/Nb and Yb (not shown), that would be expected if their Nb enrichments were derived from enriched mantle “blobs” as suggested by Castillo et al. (2002) for Philippine NEBs. The negative La/Yb versus Yb correlation displayed by the Tuotuohe NEB is most plausibly the result of mixing between batches of NEB magma and crystal fractionation and accumulation rather than variable degrees of mantle melting.

Finally, the approximately linear positive correlation between $^{147}\text{Sm}/^{144}\text{Nd}$ and $^{143}\text{Nd}/^{144}\text{Nd}$ for the Tuotuohe NEBs, magnesian andesites and adakites (Fig. 10g) also strongly suggests that they were closely related in petrogenesis (Polat and Kerrich 2002). Accordingly, we suggest that the Tuotuohe suite constitutes an adakite metasomatic arc volcanic series (Defant and Kepezhinskias 2001).

In summary, the geochronological and geochemical evidence indicates that the magnesian andesites were the product of hybridization of adakitic magmas with depleted arc mantle wedge peridotite (Defant and Kepezhinskias 2001; Polat and Kerrich 2002). The adakite melts carry far greater amounts of the HFSE than do aqueous fluids and, as established by the xenolith studies of Kepezhinskias et al. (1997), reaction of the melts with mantle peridotite produces amphibole and phlogopite, which concentrate the HFSE. These metasomatic phases are nonrefractory and break down during later mantle partial melting, resulting in magmas (i.e., NEB) with higher HFSE contents than typical arc basalts (Sajona et al. 1993, 1996; Polat and Kerrich 2002; Wyman et al. 2000; Hollings and Kerrich 2000). Experimental data suggest that adakitic magmas can only be generated in the garnet stability field (e.g., Rapp et al. 1999). The Sc-REE systematics (Fig. 10h) further indicates that the Tuotuohe adakite-magnesian andesites were produced in the garnet stability field, whereas the NEBs were possibly generated above the garnet stability field, after which the parental magmas of the NEB flows underwent crystal fractionation that included a Sc-bearing phase such as clinopyroxene (Wyman et al. 2000). The geographic association of the NEBs, magnesian andesites and adakites in the Tuotuohe area suggest that adakite-metasomatized mantle domains were not dragged away from the locus of slab melt ascent to deeper parts of the wedge by convection. Instead, decomposition of hydrous metasomatic phases probably triggered partial melting at shallower depths just above the zone of slab melting (Sajona et al. 1996; Wyman et al. 2000).

Geodynamic implications

The relative enrichment of high field strength elements (HFSE: Nb, Ta and Zr) in the Tuotuohe basalts has been equated with an intraplate mantle component that was thought to have originated in a Late Permian intracontinental rift setting (Dewey et al. 1988; Pearce and Mei 1988; Kapp et al. 2003). However our new data demonstrate that they are Middle Triassic NEBs associated with adakites and magnesian andesites, most probably in an arc setting.

Modern adakite-magnesian andesite-NEB associations are commonly associated with the subduction of young (≤ 20 –30 Ma), hot oceanic slabs (Defant et al. 1992; Defant and Kepezhinskias 2001; Kepezhinskias et al. 1996, 1997; Sajona et al. 1993, 1996; Aguilón-Robles et al. 2001). Partial melting of such slabs usually requires temperatures $>700^\circ\text{C}$ at depths of 75–85 km (Defant et al. 1992; Sajona et al. 1993; Peacock et al. 1994; Kepezhinskias et al. 1996, 1997). Recently, Gutscher et al. (2000) proposed that partial melting could also occur in moderately old (10–45 Ma) oceanic crust during the early stages of flat subduction when the leading edge of the slab is heated by ambient mantle.

It is commonly accepted that the opening of the Paleo-Tethyan ocean occurred during the Carboniferous (e.g., Dewey et al. 1988; Yin and Harrison 2000; Pan and Ding 2004). Geochronological ages of Paleo-Tethyan oceanic crust range between 329 and 231 Ma (Qu et al. 2002; Pan and Ding 2004; Jian et al. 2003; Song et al. 2004), indicating that production of new oceanic crust extended into the Late Permian–Triassic. The Nd isotopic data of the Triassic Tuotuohe adakites (Fig. 10a) suggest that they were unlikely to have originated from Carboniferous age subducted slab and were instead derived from the Late Permian–Triassic (i.e., relatively young, ≤ 30 Ma) Tethyan oceanic crust. Adakites can only occur at temperatures above 700°C and depths greater than 70–85 km, regardless of whether subduction occurs at normal dips or shallower angles (Defant et al. 1992; Sajona et al. 1993; Kepezhinskias et al. 1997; Gutscher et al. 2000). Consequently, the Paleo-Tethyan oceanic crust was likely to have subducted beneath the Qiangtang sub-arc mantle at depths of 70–85 km during the Triassic.

These findings have important implications for the tectonic evolution of Central Tibet. The presence of Triassic NEB implies a modified mantle source beneath the Qiangtang terrane while the co-existing adakites implicate a relatively deep location for the subducted slab at 220–236 Ma. In contrast, the model of Kapp et al. (2003) invokes low-angle subduction prior to 220 Ma, which they link to erosion of the deep crust in a setting devoid of an asthenospheric mantle wedge.

Our results do not entirely negate the possibility of low-angle subduction beneath the Qiangtang terrane, but they do indicate that deep crustal erosion was unlikely. It remains possible that flat subduction rapidly froze a thin asthenospheric wedge (Gutscher et al. 2000) and that scrapping off of underthrust melange occurred in response to this thickening of the non-convecting mantle. This scenario, however, remains difficult to reconcile with the Kapp et al. (2003) model, which equates the paucity of ultramafic xenoliths in the Qiangtang melange with the absence of mantle material above the slab.

In any case, our findings suggest that the deep crust of central Tibet was not dominated by a Triassic accretionary melange. Therefore, Cenozoic shoshonitic or high-K volcanic rocks in the central Qiangtang terrane are unlikely to have been generated by in situ melting of such melange as proposed by Kapp et al. (2003). The Nd isotopic compositions of the Tuotuohe NEBs indicate that the sub-arc mantle in the central Qiangtang terrane was characterized by depleted compositions (e.g., $\epsilon_{\text{ND}}(0) = 0.59\text{--}4.20$, $T_{\text{DM}} = 0.84\text{--}0.9$ Ga) at the time of basalt genesis that are distinct from the enriched mantle sources (e.g., $\epsilon_{\text{ND}}(0) = -5.95\text{--}9.09$, $T_{\text{DM}} > 0.9$ Ga) of Cenozoic volcanic rocks in the Central Qiangtang terrane (e.g., Turner et al. 1996). The modification of mantle isotopic compositions beneath the Qiangtang terrane must have occurred after generation of the NEB and may have been the product of (a) continued Triassic subduction that metasomatized a frozen asthenospheric wedge, or (b) metasomatism linked to post-Triassic tectonics such as Jurassic-Cretaceous or Cenozoic subduction (e.g., Arnaud et al. 1992; Yin and Harrison, 2000; Hacker et al. 2000; Tapponnier et al. 2001; Ding et al. 2003).

Conclusions

This study has several important implications for the understanding of Permo-Triassic tectonics of central Tibet. The concept of Permian rifting in the Qiangtang terrane (Pearce and Mei 1988; Kapp et al. 2003) was based in large part on basalts that this study shows to be at least as young as Triassic in age. Moreover, the inferred intra-plate origin of the basalts must be re-evaluated on the basis of more recent evidence of Nb-enriched rock types found in arc environments. The spatial association of the Tuotuohe NEB with adakites and magnesian andesites indicates that they are part of an “adakitic metasomatic volcanic series” recognized in many demonstrably subduction-related environments (e.g., Defant and Drummond 1990; Defant et al. 1992; Sajona et al. 1993, 1996; Kepezhinskias et al. 1996, 1997; Aguillón-Robles et al. 2001; Defant and Kepezhinskias 2001).

The 219–236 Ma ages of the Tuotuohe suite, and their likely correlation with Triassic NEB that are overlain by Norian age (206–216 Ma) fossils, indicate that volcanism derived from a subduction-modified mantle was relatively abundant prior to 220 Ma in the central Qiangtang terrane. Although these findings can be accommodated within a flat subduction scenario (Gutscher et al. 2000), they do not support the concept that flat and shallow subduction eliminated any asthenospheric wedge beneath the Qiangtang terrane in the Triassic (Kapp et al. 2003). As a corollary, tectonic erosion of the lower crust was unlikely to have been significant under much of Qiangtang terrane during this time. There are also implications for younger magmatism in the area. Cenozoic shoshonitic or high-K volcanic rocks in the central Qiangtang terrane were most likely not derived from a lower crust consisting of tectonically accreted melange. Instead, they were derived from mantle sources that were metasomatized during Triassic or younger subduction events.

Acknowledgments We sincerely thank associate editor Professor Hans Keppler and two anonymous reviewers for their constructive and helpful reviews. Professor Liu Dunyi, Tao Hua, Zhang Yuhai, Hu Shenghong, Zhu Yingtang, Pu Zhiping, Hu Guangqian, Pu Zhiping and Chen Zhenyu are thanked for their assistance with laboratory and fieldwork. We are grateful to Professor Pan Guitang and Dr. Zhu Dicheng for helpful discussions. Financial support for this research was provided by the Major State Basic Research Program of People’s Republic of China (No. 2002CB412601 and 2007CB411308), Chinese Academy of Sciences (KZCX2-YW-128 and KZCX3-SW-143:4) and the National Natural Science Foundation of China (Grant Nos. 40572042, 40425003 and 40421303), and the International Development Fund of The University of Sydney.

References

- Aguillón-Robles A, Caimus T, Bellon H, Maury RC, Cotton J, Bourgeois J, Michaud F (2001) Late Miocene adakite and Nb-enriched basalts from Vizcaino Peninsula, Mexico: indicators of East Pacific Rise subduction below southern Baja California. *Geology* 29:531–534
- Arnaud NO, Vidal Ph, Tapponnier P, Matte P, Deng WM (1992) The high K₂O volcanism of northwestern Tibet: geochemistry and tectonic implications. *Earth Planet Sci Lett* 111:351–367
- Atherton MP, Petford N (1993) Generation of sodium-rich magmas from newly underplated basaltic crust. *Nature* 362:144–146
- Boynton WV (1984) Cosmochemistry of the earth elements: meteorite studies. *Rare Earth element geochemistry*. In: Henderson R (eds) *Developments in geochemistry* 2. Elsevier, Amsterdam, pp 89–92
- Bruguier O, Lancelot JR, Malavieille J (1997) U–Pb dating on single detrital zircon grains from the Triassic Sonpan-Ganze flysch (Central China): Provenance and tectonic correlations. *Earth Planet Sci Lett* 152:217–231
- Castillo PR, Solidum RU, Punongbayan RS (2002) Origin of high field strength element enrichment in the Sulu Arc, southern Philippines, revisited. *Geology* 30:707–710
- Chung SL, Chu MF, Zhang YQ, Xie YW, Lo CH, Lee TY, Lan CY, Li XH, Zhang Q, Wang YZ (2005) Tibetan tectonic evolution

- inferred from spatial and temporal variations in post-collisional magmatism. *Earth Sci Rev* 68:173–196
- Condie KC (2003) Incompatible element ratios in oceanic basalts and komatiites: tracking deep mantle sources and continental growth rates with time. *Geochem Geophys Geosyst* 4(1):1005. doi: [10.1029/2002GC000333](https://doi.org/10.1029/2002GC000333)
- Defant MJ, Drummond MS (1990) Derivation of some modern arc magmas by melting of young subducted lithosphere. *Nature* 347:662–665
- Defant MJ, Kepezhinskas P (2001) Evidence suggests slab melting in arc magmas. *EOS* 82:62–69
- Defant MJ, Jackson TE, Drummond MS, De Boer JZ, Bellon H, Feigenson MD, Maury RC, Stewart RH (1992) The geochemistry of young volcanism throughout western Panama and southeastern Costa Rica: an overview. *J Geol Soc (London)* 149:569–579
- Dewey JF, Shackleton RM, Chang C, Sun Y (1988) The tectonic evolution of the Tibetan Plateau. *Philos Trans R Soc Lond A* 327:379–413
- Ding L, Kapp P, Zhong DL, Deng WM (2003) Cenozoic volcanic rocks in Tibet: evidence for a transition from oceanic to continental subduction. *J Petrol* 44:1833–1865
- Dungan MA, Lindstrom MM, Mmiland NJ et al. (1986) Open system magmatic evolution of the Tos Plateau volcanic field, northern New Mexico, 1. The petrology and geochemistry of the Servilleta basalt. *J Geophys Res* 91:5999–6028
- Gao S, Rudnick RL, Yuan HL, Liu XM, Liu YS, Xu WL, Lin WL, Ayers J, Wang XC, Wang QH (2004) Recycling lower continental crust in the North China craton. *Nature* 432:892–897
- Gao S, Zhang B, Gu X, Xie X, Gao C, Guo X (1995) Silurian–Devonian provenance changes of South Qinling Basin: Implications for accretion of the Yangtze (South China) to the North China Craton. *Tectonophysics* 250:183–197
- Gutscher MA, Maury R, Eissen JP, Bourdon E (2000) Can slab melting be caused by flat subduction? *Geology* 28:535–538
- Haase KM, Devey CW, Mertz DF, Stoffers P, Garbe-Schönberg D (1996) Geochemistry of lavas from Mohns Ridge, Norwegian–Greenland Sea: implications for melting conditions and magma sources near Jan Mayen. *Contrib Mineral Petrol* 123:223–237
- Hacker BR, Gnos E, Ratschbacher L, Grove M, McWilliams M, Sobolev SV, Jiang W, Wu Z (2000) Hot and dry deep crustal xenoliths from Tibet. *Science* 287:2463–2466
- Hansmann W, Oberli F (1991) Zircon inheritance in an igneous rock suite from the southern Adamello batholith (Italian Alps). *Contrib Mineral Petrol* 107:501–518
- Hofmann AW (1986) Nb in Hawaiian magmas: constraints on source composition and evolution. *Chem Geol* 57:1–17
- Hofmann AW, Jochum KP, Seufert M, White WM (1986) Nb and Pb in oceanic basalts: new constraints on mantle evolution. *Earth Planet Sci Lett* 33:33–45
- Hollings P, Kerrich R (2000) An Archean arc basalt-Nb-enriched basalt-adakite association: the 2.7 Ga confederation assemblage of the Birch-Uchi greenstone belt, Superior Province. *Contrib Mineral Petrol* 139:208–226
- Hou ZQ, Gao YF, Qu XM, Rui ZY, Mo XX (2004) Origin of adakitic intrusives generated during mid-Miocene east–west extension in southern Tibet. *Earth Planet Sci Lett* 220:139–155
- Hsü KJ, Pan GT, Sengör AMC (1995) Tectonic evolution of the Tibetan Plateau: a working hypothesis based on the Archipelago model of orogenesis. *Int Geol Rev* 37:473–508
- Hu SH, Chen AF, Lin SL, Yuan HL, Gao S (2000) Study of ICP-MS analysis of 40 trace and ultratrace elements in geological samples. *Earth Sci* 25:286–290 (in Chinese with English abstract)
- Jian P, Liu DY, Sun SM (2003) SHRIMP dating of carboniferous Jinshajiang ophiolite in western Yunnan and Sichuan: geochronological constraints on the evolution of the Paleotethys oceanic crust. *Acta Geol Sinica* 77:217–277 (in Chinese with English abstract)
- Kapp P, Yin A, Manning CE, Murphy M, Harrison TM, Spurlin M, Ding L, Deng XG, Wu CM (2000) Blueschist-bearing metamorphic core complexes in the Qiangtang block reveal deep crustal structure of northern Tibet. *Geology* 28:19–22
- Kapp P, Yin A, Manning CE, Harrison TM, Taylor MH, Ding L (2003) Tectonic evolution of the early Mesozoic blueschist-bearing Qiangtang metamorphic belt, central Tibet. *Tectonics* 22:1043. doi: [10.1029/2002TC001383](https://doi.org/10.1029/2002TC001383)
- Kay RW, Kay SM (1993) Delamination and delamination magmatism. *Tectonophysics* 219:177–189
- Kay SM, Ramos VA, Marquez M (1993) Evidence in Cerro Pampa volcanic rocks of slab melting prior to ridge trench collision in southern South America. *J Geol* 101:703–714
- Kepezhinskas PK, Defant MJ, Drummond MS (1996) Progressive enrichment of island arc mantle by melt-peridotite interaction inferred from Kamchatka xenoliths. *Geochem Cosmochim Acta* 60:1217–1229
- Kepezhinskas PK, McDermott F, Defant MJ, Hochstaedter FG, Drummond MS, Hawkesworth CJ, Koloskov A, Maury RC, Bellon H (1997) Trace element and Sr–Nd–Pb isotopic constraints on a three-component model of Kamchatka arc petrogenesis. *Geochim Cosmochim Acta* 61:577–600
- Kepler H (1996) Constraints from partitioning experiments on the composition of subduction-zone fluids. *Nature* 380:237–240
- Koppers AAP (2002) ArArCALC-software for $^{40}\text{Ar}/^{39}\text{Ar}$ age calculations. *Comput Geosci* 28(5):605–619
- Leeder MR, Smith AB, Yin JX (1988) Sedimentology and palaeoenvironmental evolution of the 1985 Lhasa to Golmud geotraverse. *Philos Trans R Soc Lond A* 327:107–143
- Li C, Cheng LR, Hu K, Zengrong Y, Hong YR (1995) Study on the paleo-Tethys suture zone of Lungmu Co-Shuanghu, Tibet Geological Publishing House, Beijing, p 131
- Li XH, Li ZX, Zhou HW, Liu Y, Kinny PD (2002) U–Pb zircon geochronology, geochemistry and Nd isotopic study of Neoproterozoic bimodal volcanic rocks in the Kangdian Rift of south China: implications for the initial rifting of Rodinia. *Precambrian Res* 113:135–154
- Martin H (1999) Adakitic magmas: modern analogues of Archaean granitoids. *Lithos* 46:411–429
- Niu YL, Batiza R (1997) Trace element evidence from seamounts for recycled oceanic crust in the Eastern Pacific mantle. *Earth Planet Sci Lett* 148:471–483
- Pan GT, and Ding J (2004) The geological map (1:1, 500, 000) of the Tibetan Plateau and neighbouring area and its specification. Map Publishing House, Chengdu, pp 1–133 (in Chinese with English abstract)
- Peacock SM, Rushmer T, Thompson AB (1994) Partial melting of subducting oceanic crust. *Earth Planet Sci Lett* 121:227–244
- Pearce JA, Mei H (1988) Volcanic rocks of the 1985 Tibet geotraverse: Lhasa to Golmud. *Philos Trans R Soc Lond A* 327:169–201
- Polat A, Kerrich R (2002) Nd-isotope systematics of ~2.7 Ga adakites, magnesian andesites, and arc basalts, Superior Province: evidence for shallow crustal recycling at Archean subduction zones. *Earth Planet Sci Lett* 202:345–360
- Puchtel IS, Haase KM, Hofmann AW, Chauvel C, Kulikov VS, Garbe-Schönberg CD, Nemchin AA (1997) Petrology and geochemistry of crustally contaminated komatiitic basalts from the Vetryny Belt, southeastern Baltic Shield: evidence for an early Proterozoic mantle plume beneath rifted Archean continental lithosphere. *Geochim Cosmochim Acta* 61:1205–1222
- Qiu HN (2006) Construction and development of new Ar–Ar laboratories in China: Insight from GV-5400 Ar–Ar laboratory

- in Guangzhou Institute of Geochemistry, Chinese Academy of Sciences. *Geochimica* 35(2):133–140 (in Chinese with English abstract)
- Qiu HN, Jiang YD (2007) Sphalerite $^{40}\text{Ar}/^{39}\text{Ar}$ progressive crushing and stepwise heating techniques. *Earth Planet Sci Lett* 256:224–232
- Qu X, Hou Z (2002) $^{40}\text{Ar}/^{39}\text{Ar}$ age of the Panyong pillow basalt: Implication for the evolution relationship between the Jinshajiang and Gaze-Litang suture zones. *Geol Rev* 48(Supp.):115–121 (In Chinese with English abstract)
- Rapp RP, Shimizu N, Norman MD, Applegate GS (1999) Reaction between slab-derived melts and peridotite in the mantle wedge: Experimental constraints at 3.8 GPa. *Chem Geol* 160:335–356
- Roger F, Arnaud N, Gilder S, Tapponnier P, Jolivet M, Brunel M, Malavieille J, Xu Z, Yang J (2003) Geochronological and geochemical constraints on Mesozoic suturing in east central Tibet. *Tectonics* 22:1037. doi:10.1029/2002TC001466
- Rudnick RL, Gao S (2003) Composition of the continental crust. In: Rudnick RL (ed) *The crust vol 3 Treatise on geochemistry* (eds Holland HD, Turekian KK) [M]. Elsevier, Oxford, pp 1–64
- Sajona FG, Maury RC, Bellon H, Cotton J, Defant MJ, Pubellier M, Rangin C (1993) Initiation of subduction and the generation of slab melts in western and eastern Mindanao, Philippines. *Geology* 21:1007–1010
- Sajona FG, Maury RC, Bellon H, Cotton J, Defant M (1996) High field strength element enrichment of Pliocene–Pleistocene island arc basalts, Zamboanga Peninsula, western Mindanao (Philippines). *J Petrol* 37:693–726
- Sha JG (1998) Characteristics of stratigraphy and palaeontology of Hohxil, Qinghai: geographic significance. *Acta Palaeontologica Sinica* 37:85–95 (In Chinese with English abstract)
- Song XY, Zhou MF, Cao ZM, Robinson PT (2004) Late Permian rifting of the South China Craton caused by the Emeishan mantle plume? *J Geol Soc Lond* 161:773–781
- Sun SS, McDonough WF (1989) Chemical and isotopic systematics of oceanic basalts: implications for mantle composition and processes. In: Saunders AD, Norry MJ (eds) *Implications for mantle composition and processes, magmatism in the ocean Basins*. Geological Society, London, Special publication vol 42, pp 313–345
- Tapponnier P, Xu ZQ, Roger F, Meyer B, Arnaud N, Wittlinger G, Yang JS (2001) Oblique stepwise rise and growth of the Tibet plateau. *Science* 294:1671–1677
- Turner S, Arnaud N, Liu J, Rogers N, Hawkesworth C, Harris N, Kelley S, van Calsteren P, Deng W (1996) Postcollision, shoshonitic volcanism on the Tibetan plateau: Implications for convective thinning of the lithosphere and the source of ocean island basalts. *J Petrol* 37:45–71
- Wang Q, McDermott F, Xu JF, Bellon H, Zhu YT (2005) Cenozoic K-rich adakitic volcanic rocks in the Hohxil area, northern Tibet: lower-crustal melting in an intracontinental setting. *Geology* 33:465–468
- Wang Q, Wyman DA, Zhao ZH, Xu JF, Bai ZH, Xiong XL, Dai TM, Li CF, Chu ZY (2007a) Petrogenesis of Carboniferous adakites and Nb-enriched arc basalts in the Alataw area, northern Tianshan Range (western China): Implication for Phanerozoic crustal growth of Central Asia Orogenic Belt. *Chem Geol* 236:42–64
- Wang Q, Wyman DA, Xu JF, Jian P, Zhao ZH, Li CF, Xu W, Ma JL, He B (2007b) Early Cretaceous adakitic granites in the Northern Dabie complex, central China: implications for partial melting and delamination of thickened lower crust. *Geochim Cosmochim Acta* 71:2609–2636
- Wijbrans JR, Pringle MS, Koppers AAP, Scheveers R (1995) Argon geochronology of small samples using the vulkaan argon laserprobe. *Proc K Ned Akad Wet: Biol Chem Geol Phys Med Sci* 98:185–218
- Wyman DA, Ayer JA, Devaney JR (2000) Niobium-enriched basalts from the Wabigoon subprovince, Canada: evidence for adakitic metasomatism above an Archean subduction zone. *Earth Planet Sci Lett* 179:21–30
- Xu JF, Castillo PR (2004) Geochemical and Nd–Pb isotopic characteristics of the Tethyan asthenosphere: implications for the origin of the Indian Ocean mantle domain. *Tectonophysics* 393:9–27
- Xu JF, Shinjio R, Defant MJ, Wang Q, Rapp RP (2002) Origin of Mesozoic adakitic intrusive rocks in the Ningzhen area of east China: partial melting of delaminated lower continental crust? *Geology* 30:1111–1114
- Yin A, Harrison TM (2000) Geologic evolution of the Himalayan–Tibetan orogen. *Annu Rev Earth Planet Sci* 28:211–280
- Yogodzinski GM, Volynets ON, Koloskov AV, Seliverstov NI (1994) Magnesian andesites and the subduction component in a strongly calcalkaline series at Piip Volcano, far western Aleutians. *J Petrol* 34:163–204
- Zhang KJ (2001) Blueschist-bearing metamorphic core complexes in the Qiangtang block reveal deep crustal structure of northern Tibet: comment. *Geology* 29:90
- Zhang YF, Zheng JK (1994) The geological outline on the Hoh Xil and its adjacent region. Seismological Press, Beijing, Pp 1–177 (in Chinese with English abstract)
- Zhang HF, Sun M, Zhou XH (2002) Mesozoic lithosphere destruction beneath the North China Craton: evidence from major-, trace elements and Sr–Nd–Pb isotope studies of Fangcheng basalts. *Contrib Mineral Petrol* 144:241–253
- Zhang KJ, Zhang YX, Li B, Zhu YT, Wei RZ (2006a) The blueschist-bearing Qiangtang metamorphic belt (northern Tibet, China) as an in situ suture zone: evidence from geochemical comparison with the Jinsa suture. *Geology* 34:493–496
- Zhang KJ, Cai JX, Zhang YX, Zhao TP (2006b) Eclogites from central Qiangtang, northern Tibet (China) and tectonic implications. *Earth Planet Sci Lett* 245:722–729
- Zhou MF, Yan DP, Wang CL, Qi L, Kennedy A (2006) Subduction-related origin of the 750 Ma Xuelongbao adakitic complex (Sichuan Province, China): implications for the tectonic setting of the giant Neoproterozoic magmatic event in South China. *Earth Planet Sci Lett* 248:286–300